Characterization and Receiver Design for Underwater Acoustic Channels with Large Doppler Spread

Qin Lu†, Yi Huang†, Zhaohui Wang‡, and Shengli Zhou†
†Dept. of Electrical and Computer Engineering, University of Connecticut, Storrs, CT, USA
‡Dept. of Electrical and Computer Engineering, Michigan Technological University, Houghton, MI, USA

***Abstract*—A time-varying underwater acoustic channel consists of multiple propagation paths which could have drastically distinct Doppler scaling factors. For example, in a communication scenario with mobile nodes, some paths might experience positive Doppler scales while others have negative Doppler scales, leading to a large Doppler spread. In this work, we address two issues. First, we quantify the channel Doppler spread of an underwater acoustic channel based on the instantaneous channel estimate from a probing signal. Second, we develop an OFDM receiver specifically for channels with large Doppler spread. Data sets collected from a swimming pool with a moving node are used for channel characterization and performance evaluation.**

***Index Terms*—Underwater acoustic channels, Doppler spread, channel estimation, data detection.**

I. Introduction

The past decade has witnessed rapid development of underwater acoustic communications for both single-carrier and multi-carrier schemes. Underwater acoustic channels are drastically different from wireless radio channels in that different propagation paths could have distinct Doppler scaling factors, leading to a large Doppler spread. A receiver front-end with multiple resampling branches is proposed in [1] for channels with large Doppler spread. Two iterative receivers are developed in [2] for distributed multi-input multi-output OFDM systems where the channels corresponding to different transmitters have different Doppler scales.

Data sets collected from sea experiments with stationary transceivers might not reveal channels with a large Doppler spread. In this paper, we focus on experiments in swimming pools with a moving node at different speeds. Fig. 1 shows convincing examples of channels with different Doppler scaling factors on different paths.

In this paper, we address two important issues. First, we present a method to quantize the channel condition by estimating the channel delay spread and Doppler spread. This is done based on the instantaneous channel estimate using a probing signal. Based on the estimated Doppler spread, the multipath channels are classified into different categories. Channels in different categories lead to different levels of intercarrier interference (ICI) for an orthogonal-frequency-division-multiplexing (OFDM) transmission.

Second, we present an OFDM receiver that combines the strengths of the Markov Chain Monte Carlo (MCMC) based data detection [3] with that of sparse channel estimation methods [4]. As in [3], each sample sequence could be associated with its own channel estimate for improved performance at the expense of receiver complexity. The receiver performance is tested on channels with different ranges of Doppler spreads.

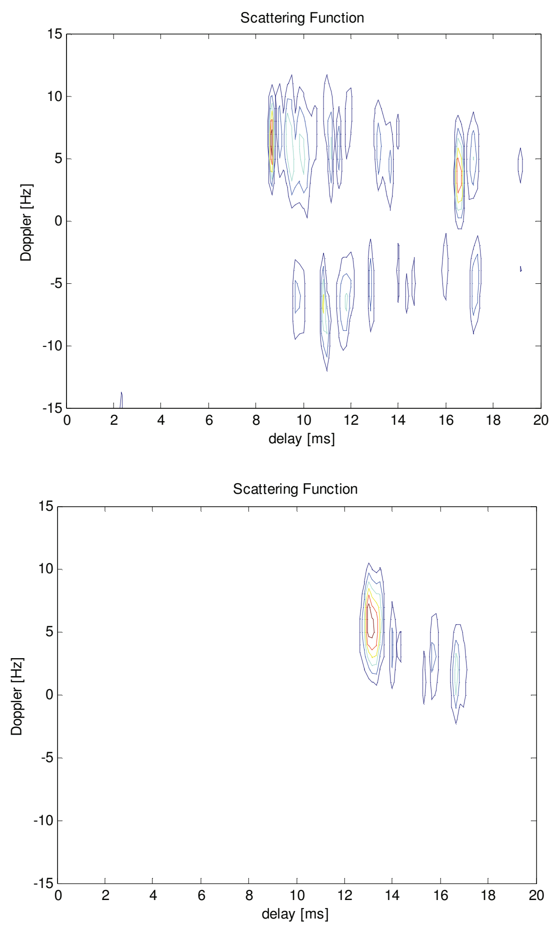

Fig. 1. Two examples of underwater acoustic channels, where different paths have different Doppler scales.

The rest of the paper is organized as follows. Section II describes the system model. Channel categorization is presented in Section III and the receiver design is detailed in Section IV. Finally, conclusions are contained in Section V.

978-0-933957-43-5 ©2015 MTS

II. System Model

The system model as in [4], [5] will be presented here. Consider a zero-padded OFDM block. Let B be the bandwidth and K be the number of subcarriers. The subcarrier spacing is thus $\Delta f = B/K$, and the time duration of one OFDM symbol is $T = 1/(\Delta f) = K/B$. After appending a guard interval of length T_{g}, the total duration of one OFDM block is $T_{\mathrm{bl}} = T + T_{\mathrm{g}}$. The kth subcarrier frequency is

$$f_k = f_{\mathrm{c}} + k\Delta f, \quad k = -K/2, ..., K/2 - 1 \tag{1}$$

where f_{c} is center frequency. The K subcarriers are divided into three sets: data subcarrier set $\mathcal{S}_{\mathrm{D}}$ for data transmission, pilot subcarrier set $\mathcal{S}_{\mathrm{P}}$ for channel estimation, and null subcarrier set $\mathcal{S}_{\mathrm{N}}$ for noise estimation, which satisfy $\mathcal{S}_{\mathrm{D}} \bigcup \mathcal{S}_{\mathrm{P}} \bigcup \mathcal{S}_{\mathrm{N}} = \{-K/2, ...K/2-1\}$. Let $s[k]$ denote the information symbol to be transmitted on the kth subcarrier. The transmitted signal is given by

$$\tilde{x}(t) = 2\mathrm{Re}\left\{\left[\sum_{k\in\mathcal{S}_{\mathrm{D}}\bigcup\mathcal{S}_{\mathrm{P}}} s[k]e^{j2\pi\frac{k}{T}t}g(t)\right]e^{j2\pi f_{\mathrm{c}}t}\right\}, \quad t \in [0, T+T_{\mathrm{g}}] \tag{2}$$

where $g(t)$ is a rectangular pulse shaper with unit value when $t \in [0, T]$ and zero elsewhere.

A time-varying underwater acoustic channel is characterized by N_{pa} triplets $\{A_p, \tau_p, a_p\}$, where N_{pa} denotes the number of paths, and A_p, τ_p, a_p represent the amplitude, the initial delay, and the Doppler scaling factor of the pth path, respectively. The channel impulse response (CIR) is given by

$$h(\tau, t) = \sum_{p=1}^{N_{\mathrm{pa}}} A_p\delta(\tau - [\tau_p - a_p t]). \tag{3}$$

After passing through the channel in (3), the received passband signal is

$$\tilde{y}(t) = \sum_{p=1}^{N_{\mathrm{pa}}} A_p\tilde{x}([1+a_p]t - \tau_p) + \tilde{w}(t) \tag{4}$$

where $\tilde{w}(t)$ is the additive noise. The receiver applies a two-step procedure to mitigate the predominant channel Doppler effect: resampling operation using a rough Doppler scale estimate $\hat{a}$ and residual Doppler shift compensation by $e^{-j2\pi\hat{\epsilon}}$ [4], where $\hat{\epsilon}$ is the estimated carrier frequency offset. The signal after preprocessing is $\tilde{z}(t) = \tilde{y}(t/(1+\hat{a}))e^{-j2\pi\hat{\epsilon}t}$. The frequency domain measurement on the mth subcarrier is then

$$\begin{aligned} z[m] &= \int_0^{T_{\mathrm{bl}}} \tilde{z}(t)e^{-j2\pi f_m t}dt \\ &= \sum_{k=-K/2}^{K/2-1} H[m,k]s[k] + w[m] \end{aligned} \tag{5}$$

where $H[m, k]$ is the ICI coefficient which specifies the contribution of the symbol on the kth subcarrier to the measurement on the mth subcarrier, which can be represented as [4]

$$H[m,k] = \sum_{p=1}^{N_{\mathrm{pa}}} \xi_p e^{-j2\pi\frac{m}{T}\bar{\tau}_p} G\left(\frac{f_m + \hat{\epsilon}}{1+b_p} - f_k\right), \tag{6}$$

where $G(f)$ is Fourier transform of $g(t)$, and ξ_p, $\bar{\tau}_p$, b_p are the complex gain, the scaled delay, and the residual Doppler rate of the pth path, respectively,

$$b_p = \frac{a_p - \hat{a}}{1+\hat{a}}, \quad \bar{\tau}_p = \frac{\tau_p}{1+b_p}, \quad \xi_p = \frac{A_p}{1+b_p}e^{-j2\pi\frac{m}{T}\bar{\tau}_p}. \tag{7}$$

Define a $K \times K$ diagonal matrix $\mathbf{\Lambda}$ with the mth diagonal element $[\mathbf{\Lambda}(\tau)]_{m,m} = e^{-j2\pi\frac{m}{T}}\tau$, and another $K \times K$ matrix $\mathbf{\Gamma}$ with the (m, k)th element $[\mathbf{\Gamma}(b, \epsilon)]_{m,k} = G\left(\frac{f_+\epsilon}{1+b} - f_k\right)$, the channel mixing matrix can be expressed as

$$\mathbf{H} = \sum_{p=1}^{N_{\mathrm{pa}}} \xi_p\mathbf{\Lambda}(\bar{\tau}_p)\mathbf{\Gamma}(b_p, \hat{\epsilon}). \tag{8}$$

The matrix-vector representation of (5) is

$$\mathbf{z} = \mathbf{Hs} + \mathbf{w}, \tag{9}$$

where $\mathbf{z}$, $\mathbf{s}$, and $\mathbf{w}$ are the vectors containing the frequency-domain samples, the transmitted symbols, and the additive noise.

III. Channel Characterization

Reconstruction of the channel mixing matrix in (8) needs the estimates of the N_{pa} path triplets $\{\xi_p, \bar{\tau}_p, b_p\}$. Following the approach in [4], an overcomplete dictionary for $\{\bar{\tau}_p, b_p\}$ can be constructed from the uniformly spaced grids:

$$\bar{\tau}_p \in \{0, \frac{T}{\lambda K}, \frac{2T}{\lambda K}, ..., T_{\mathrm{g}}\} \tag{10}$$

$$b_p \in \{-b_{\max}, -b_{\max} + \Delta b, ..., b_{\max}\} \tag{11}$$

where T/K is the sampling interval in baseband, λ is the oversampling factor, $b_{\max}$ is the maximum Doppler scale to be searched and Δb is the step size. In total, there are $N_1 = \lambda K T_{\mathrm{g}}/T$ tentative delays and $N_2 = 2b_{\max}/\Delta b + 1$ tentative Doppler scales. Although $N_1 N_2$ candidate paths will be searched, only a few of them will be nonzero due to the sparse nature of underwater acoustic channels.

Define a vector $\boldsymbol{\xi}_i = [\xi_{1,i}, ..., \xi_{N_1,i}]^T$ to contain the path gains with the same Doppler rate b_i, and stack $\{\boldsymbol{\xi}_i\}$ into a long vector as $\mathbf{x} = [\boldsymbol{\xi}_1^T, ..., \boldsymbol{\xi}_{N_2}^T]^T$. Combining all $N_1 N_2$ candidate paths, the input-output relationship can be rewritten as

$$\mathbf{z} = \sum_{l=1}^{N_1}\sum_{i=1}^{N_2} \xi_{l,i}\mathbf{\Lambda}(\bar{\tau}_l)\mathbf{\Gamma}(b_i, \hat{\epsilon})\mathbf{s} + \mathbf{w} = \mathbf{Ax} + \mathbf{w} \tag{12}$$

where

$$\mathbf{A} = [\mathbf{\Lambda}(\bar{\tau}_1)\mathbf{\Gamma}(b_1, \hat{\epsilon})\mathbf{s}, ..., \mathbf{\Lambda}(\bar{\tau}_{N_1})\mathbf{\Gamma}(b_{N_2}, \hat{\epsilon})\mathbf{s}]. \tag{13}$$

The symbol vector $\mathbf{s}$ for the probing signal is known at the receiver. With the constraint that $\mathbf{x}$ is sparse, the channel estimation problem is formulated as:

$$\hat{\mathbf{x}} = \arg\min_{\mathbf{x}} \frac{1}{2}\|\mathbf{z} - \mathbf{Ax}\|_2^2 + \lambda\|\mathbf{x}\|_q^q, \tag{14}$$

where λ is the sparsity factor. For different choices of q, different sparse recovery algorithms have been studied and compared in [6] for channel estimation in underwater OFDM.

The estimated number of paths $\hat{N}_{\rm pa}$ is the number of nonzero entries in $\hat{\mathbf{x}}$. Based on (7), the Doppler scale $\hat{a}_p$, the delay $\hat{\tau}_p$ and the magnitude $|\hat{A}_p|$ for the pth path are:

$$\hat{a}_p = \hat{a} + (1+\hat{a})\hat{b}_p, \tag{15}$$

$$\hat{\tau}_p = (1+\hat{b}_p)\hat{\bar{\tau}}_p, \tag{16}$$

$$|\hat{A}_p| = (1+\hat{b}_p)|\hat{\xi}_p|. \tag{17}$$

A. Channel Classification

The average values of the delays and Doppler scales are

$$\hat{\tau}_{\rm mean} = \sum_{p=1}^{\hat{N}_{\rm pa}} |\hat{A}_p|^2 \hat{\tau}_p, \tag{18}$$

$$\hat{a}_{\rm mean} = \sum_{p=1}^{\hat{N}_{\rm pa}} |\hat{A}_p|^2 \hat{a}_p. \tag{19}$$

The delay spread and Doppler spread are estimated as

$$\hat{\tau}_{\rm spread} = \sum_{p=1}^{\hat{N}_{\rm pa}} |\hat{A}_p|^2 (\hat{\tau}_p - \hat{\tau}_{\rm mean})^2, \tag{20}$$

$$\hat{a}_{\rm spread} = \sum_{p=1}^{\hat{N}_{\rm pa}} |\hat{A}_p|^2 (\hat{a}_p - \hat{a}_{\rm mean})^2. \tag{21}$$

In short, the instantaneous squared amplitudes are used to weight the delay and Doppler values, in the absence of statistic information. Such a use can be also found in e.g., [7].

B. Pool Data

Data sets collected from a swimming pool are used for channel characterization. The system parameters are as follows: bandwidth $B = 6$ kHz, center frequency $f_{\rm c} = 17$ kHz and subcarrier spacing $\Delta f = 5.9$ Hz. There are $K = 1024$ subcarriers, out of which 256 are data subcarriers, 96 are null subcarriers and 672 are data subcarriers. QPSK constellation and rate $1/2$ nonbinary LDPC coding over GF(4) are used. In the tests, we keep one node moving at different speeds. Due to the special environment of the swimming pool, we can observe distinct Doppler scaling factors in different paths and in most cases both positive and negative Doppler scales are present in the mobile scenario, leading to a large Doppler spread.

The data blocks are assumed known for channel estimation, where we use the orthogonal matching pursuit (OMP) algorithm with 40 iterations; i.e., 40 paths are extracted. Fig. 2 shows an example of the channel estimate on top of the channel scattering function.

Now classify the channels based on 156 data blocks collected. Convert the Doppler spread to have the unit in Hertz as $f_{\rm Dop} = \hat{a}_{\rm spread} f_{\rm c}$, and then separate the data blocks into the following four groups:

- Doppler spread $[0,\, 0.2\Delta f]$ Hz

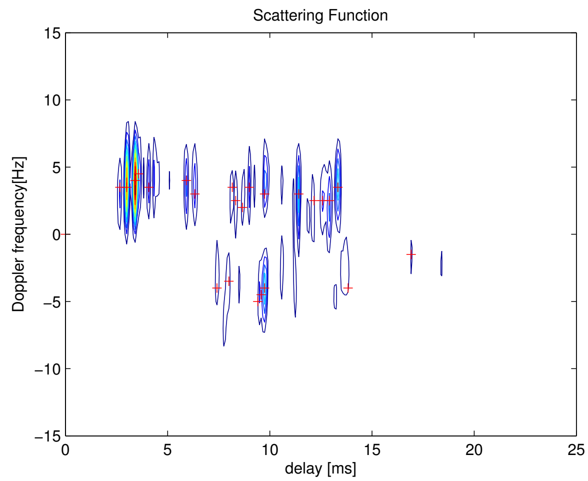

Fig. 2. An estimated channel on top of the scattering plot

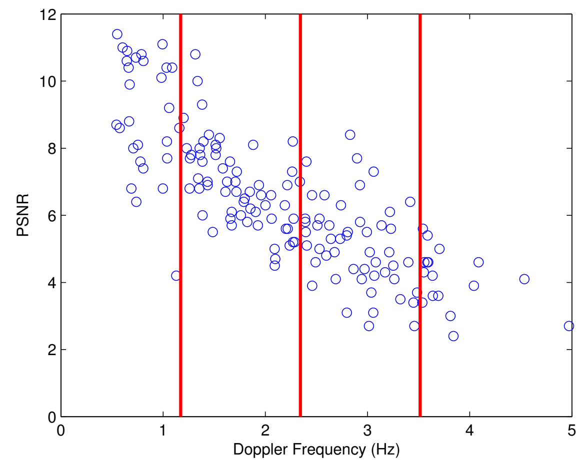

Fig. 3. PSNR *vs* the estimated Doppler spread for pool test data

- Doppler spread $[0.2\Delta f,\, 0.4\Delta f]$ Hz
- Doppler spread $[0.4\Delta f,\, 0.6\Delta f]$ Hz
- Doppler spread $[0.6\Delta f,\, \Delta f]$ Hz

There are 28, 61, 50 and 17 blocks for each group, respectively.

The pilot signal-to-noise ratio (PSNR) of each block can be measured as the ratio of the energy on the pilot subcarriers to the energy on the null subcarriers. Fig. 3 shows the PSNR values of all the blocks corresponding to the estimated Doppler spreads. Clearly, PSNR tends to decrease as the Doppler spread increases. Next, define the normalized ICI power on the dth ($d \in \{\pm 1, \pm 2, \dots\}$) neighboring subcarriers as

$$\mathrm{ICI}(d) = \frac{\sum_m |\hat{H}[m, m+d]|^2}{\sum_m |\hat{H}[m,m]|^2}. \tag{22}$$

Fig. 4 shows the average normalized ICI power with respect to the offset d for different groups of channel. Finally, assume that the receiver can handle ICI within a depth D, and treat the ICI from distant neighbors as additive noise, the signal-to-ICI

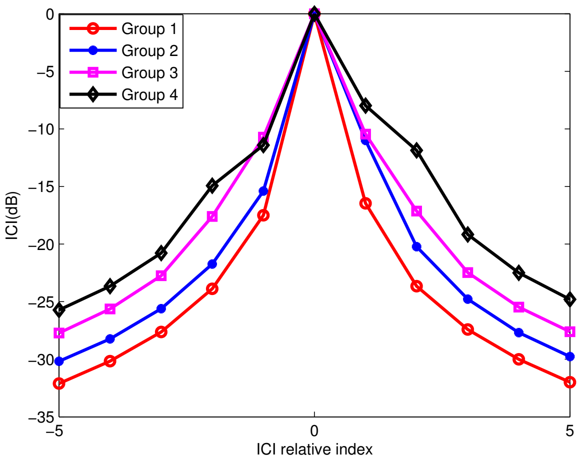

Fig. 4. The normalized ICI power as a function of subcarrier offset d

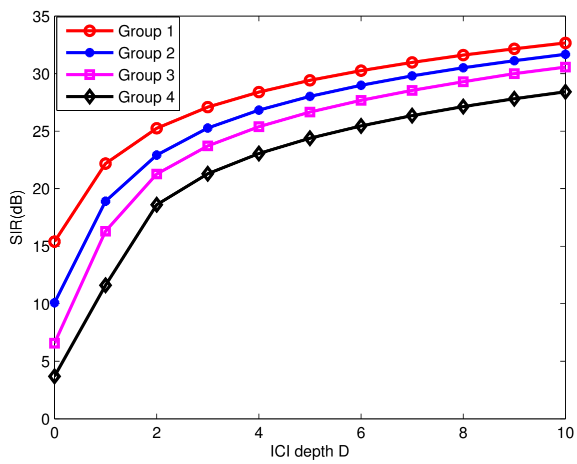

Fig. 5. SIR as a function of the ICI depth D

ratio (SIR) can be defined as

$$\mathrm{SIR}(D) = \frac{\mathbb{E}_{m \in \mathcal{S}_{\rm all}} \left[\sum_{k:|k-m| \le D} |\hat{H}[m,k]|^2 \right]}{\mathbb{E}_{m \in \mathcal{S}_{\rm all}} \left[\sum_{k:|k-m| > D} |\hat{H}[m,k]|^2 \right]}. \tag{23}$$

Fig. 5 plots the SIR as a function of the ICI depth D for different groups. Figs. 4 and 5 confirm that the ICI becomes more dominant as the Doppler spread increases.

IV. Receiver Design for Channels with Large Doppler Spread

We now consider the receiver design to decode the data blocks. Ref. [5] has proposed an iterative receiver for underwater acoustic channels with small to moderate Doppler spread where channel estimation and data detection are coupled. In each iteration, sparse channel estimation is carried out, followed by data detection in the presence of ICI. Three ICI equalizers: MAP, MMSE, and MCMC equalizers, have been explored.

In this paper, we explore the receiver, MCMC with list channel estimates (MCMC-LCE), originally proposed in [3] for single carrier transmissions over time-varying underwater acoustic channels. This approach differs from the traditional MCMC detector in that the channel estimate is updated every time a new sample is drawn. Thus, a list of samples and their corresponding channel estimates is formed, based on which the extrinsic log-likelihood ratio (LLR) is computed and then fed into the channel decoder. The effectiveness of the MCMC-LCE equalizer has been validated using both synthetic channels and experimental data for single carrier transmissions in [3]. Here, we would like to apply this principle to underwater OFDM to mitigate the intercarrier interference over channels with large Doppler spread.

The procedure of the MCMC-LCE receiver using sparse channel estimation is summarized in Algorithm 1. Since there is no bit-to-symbol and symbol-to-bit conversion in our system, symbol-wise Gibbs sampler is employed. We consider $N_{\rm g}$ parallel Gibbs samplers (GS) and each Gibbs sampler runs $N_{\rm s}$ iterations. The initial sample $\mathbf{s}^{(0)}$ of each Gibbs sampler is generated based on $\boldsymbol{\lambda}^e$, the extrinsic information provided by the channel decoder. During the nth iteration, we sequentially update the symbols on the data subcarriers based on the sample $\mathbf{s}^{(n-1)}$ and channel estimates $\hat{\mathbf{H}}^{(n-1)}$ from the previous iteration. The a posterior probability (APP) of the mth entry of $\mathbf{s}^{(n)}$, denoted as $s_m^{(n)}$, is updated according to

$$\begin{aligned} &\Pr(s_m^{(n)} = a_i | \mathbf{z}, \bar{\mathbf{s}}_m^{(n)}, \hat{\mathbf{H}}^{(n-1)}, \boldsymbol{\lambda}^{\rm e}) \\ &\quad \propto \Pr(\mathbf{z} | \bar{\mathbf{s}}_m^{(n)}, s_m^{(n)} = a_i, \hat{\mathbf{H}}^{(n-1)}) \Pr(s_m^{(n)} = a_i | \boldsymbol{\lambda}^{\rm e}) \\ &\quad = \exp\left(- \frac{\| \mathbf{z} - \hat{\mathbf{H}}^{(n-1)} \bar{\mathbf{s}}_{m,a_i}^{(n)} \|^2}{\hat{N}_0} \right) \Pr(s_m^{(n)} = a_i | \boldsymbol{\lambda}^{\rm e}) \end{aligned} \tag{24}$$

where $\bar{\mathbf{s}}_m^{(n)} = \left[s_1^{(n)}, ..., s_{m-1}^{(n)}, s_{m+1}^{(n-1)}, ..., s_K^{(n-1)} \right]$, $\bar{\mathbf{s}}_{m,a_i}^{(n)} = \left[s_1^{(n)}, ..., s_{m-1}^{(n)}, a_i, s_{m+1}^{(n-1)}, ..., s_K^{(n-1)} \right]$, $\hat{N}_0$ is the estimated noise variance, a_i, $(i = 1, ..., M)$, is the ith point in the constellation and M is the constellation size.

Due to the high complexity of the sparse channel estimation algorithm for OFDM, the channel estimate is updated every $N_{\rm up}$ samples. If $N_{\rm up}$ is larger than N_s, the proposed MCMC-LCE receiver becomes the MCMC receiver considered in [5]. Considering the large size of $\hat{\mathbf{H}}^{(n)}$ (1024×1024 in our system), we do not save the list $\{\mathbf{s}^{(n)}, \hat{\mathbf{H}}^{(n)}\}$. Instead, we form the list $\{\mathbf{s}^{(n)}, \boldsymbol{\beta}^{(n)}\}$ contributed by $\hat{\mathbf{H}}^{(n)}$. The (m, i)th entry of $\boldsymbol{\beta}^{(n)}$ is given by

$$\begin{aligned} \beta_{m,i}^{(n)} &= \Pr(\mathbf{z} | \mathbf{s}_{m,a_i}^{-(n)}, \hat{\mathbf{H}}^{(n)}) \Pr(\boldsymbol{\lambda}^{\rm e}) \\ &= \exp\left(- \frac{\| \mathbf{z} - \hat{\mathbf{H}}^{(n)} \mathbf{s}_{m,a_i}^{(-n)} \|^2}{\hat{N}_0} \right) \Pr(\boldsymbol{\lambda}^{\rm e}), \end{aligned} \tag{25}$$

where $\mathbf{s}_{m,a_i}^{-(n)} = \left[s_1^{(n)}, ..., s_{m-1}^{(n)}, a_i, s_{m+1}^{(n)}, ..., s_K^{(n)} \right]$.

Finally, the LLR vector for each symbol on the data subcarriers is calculated along the max-log-MAP principle as

$$\lambda_{m,i} = \ln \frac{\max\{\beta_{m,i}^{(n)}\}_{n=1}^{\Omega}}{\max\{\beta_{m,1}^{(n)}\}_{n=1}^{\Omega}}, \tag{26}$$

Algorithm 1 : MCMC-LCE with sparse channel estimation

Step 1: Sequentially draw samples and update channel estimates every several samples
for $g = 1 : N_{\mathrm{g}}$ **do**
  generate an initial sample $\mathbf{s}^{(0)}$ according to $\boldsymbol{\lambda}^{\mathrm{e}}$;
  for $n = 1 : N_{\mathrm{s}}$ **do**
    for $m \in \mathcal{S}_{\mathrm{D}}$ **do**
      Calculate $\{P(s_m^{(n)} = a_i | \mathbf{z}, \bar{\mathbf{s}}_m^{(n)}, \hat{\mathbf{H}}^{(n-1)})\}_{i=1}^{M}$ using (24) and then generate $s_m^{(n)}$;
    end for

    if $\mathrm{rem}(n, N_{\mathrm{up}}) = 0$ **then**
      Update channel estimate $\hat{\mathbf{H}}^{(n)}$;
    else
      $\hat{\mathbf{H}}^{(n)} = \hat{\mathbf{H}}^{(n-1)}$;
    end if

    Calculate the contribution of $\{\mathbf{s}^{(n)}, \hat{\mathbf{H}}^{(n)}\}$ as in (25) and put $\{\mathbf{s}^{(n)}, \boldsymbol{\beta}^{(n)}\}$ into the list;
  end for
end for

Step 2: Calculate the LLRs according to (26).

where Ω is the number of samples.

A. Simulation Results

The OFDM system parameters are the same as in the data in the pool test. To obtain channels with large Doppler spread, we generate 10 paths with distinct Doppler speeds $v = ac$, of which 5 are drawn from a normal distribution with positive mean $\bar{v}_1 = 0.5$ m/s and the rest 5 have a negative mean $\bar{v}_2 = -0.5$ m/s. The two distributions have the same standard deviation as $\sigma_v = 0.1$ m/s. The inter-arrival times are distributed exponentially with mean 1 ms, leading to a total average delay of 10 ms. A total of 1000 received data blocks are generated, and the average Doppler frequency is 3.88 Hz for the 1000 blocks.

As in [5], the SpaRSA algorithm from [8] is used for channel estimation at the receiver. In the initial round, data symbols are unknown, and measurements on the data subcarriers are excluded. Later, channel estimation is carried out based on the individual symbol sequence in the MCMC-LCE receiver. To simplify the receiver implementation, the ICI beyond the depth $D = 3$ is ignored, i.e., $\hat{H}[m, k]$ is set to zero when $|m - k| > D$.

For the fairness of comparison, the same size of Gibbs sampler, 1 Gibbs sampler with 20 samples, will be utilized for both the MCMC and MCMC-LCE receivers. The channel estimate is updated every 5 samples for the MCMC-LCE receiver. Fig. 6 shows the block error rate (BLER) of the proposed MCMC-LCE receiver compared with that of the original MCMC receiver for different numbers of iterations. As seen from Fig. 6, the MCMC-LCE receiver has a performance

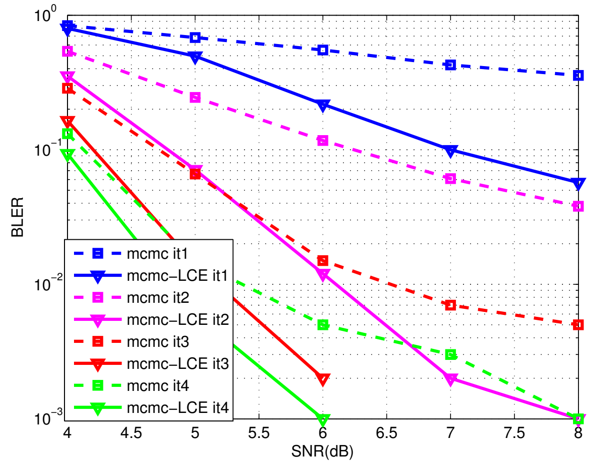

Fig. 6. Simulated BLER performance

gain of 2 dB over the original MCMC receiver when the BLER is 10^{-3} at the 4th iteration.

B. Experimental Results

We have classified the pool test data into 4 groups based on the estimated Doppler spread. Now we would like to see how MCMC-LCE and MCMC receivers behave for different groups of data. Each receiver has five iterations.

Table I summarizes the number of decoded data blocks within each group for different ICI depths using the MCMC or MCMC-LCE receivers ($D = 1, 2, 3, 4, 5, 10$). Fig. 7 shows the average BLER of the data blocks within each group for MCMC and MCMC-LCE receivers, with $D = 3$. Since the BLER performance is rather poor for single block decoding, we have also explored the performance of block combining for blocks within each group, as all the blocks correspond to the same transmit OFDM symbol. We randomly choose up to 100 combinations and obtain the BLER within each group. Using $D = 3$, Figs. 8 and 9 show the BLERs for the MCMC and MCMC-LCE receivers, when combining two and four blocks, respectively.

From Table I, Figs. 7 and 9, we have the following observations. When the Doppler frequency is small (for data blocks in group 1), the MCMC receiver slightly outperforms the MCMC-LCE receiver. However, as Doppler frequency increases, MCMC-LCE becomes better than MCMC. When the Doppler spread is small, the uncoded BER will be rather small, which means that the sequence from the channel decoder is almost correct and hence the corresponding channel estimate would be good. As a result, the MCMC receiver can achieve good performance. When Doppler spread is large, the MCMC-LCE receiver is helpful by updating the channel estimates for different symbol sequences. Obviously, the channels with large Doppler spread are challenging, and multi-block combining (receiver diversity) can greatly improve the decoding performance.

TABLE I
SUCCESSFULLY DECODED BLOCKS FOR MCMC AND MCMC-LCE RECEIVERS WITH DIFFERENT ICI DEPTHS

	MCMC						MCMC-LCE					
	$D=1$	$D=2$	$D=3$	$D=4$	$D=5$	$D=10$	$D=1$	$D=2$	$D=3$	$D=4$	$D=5$	$D=10$
Group 1 (28 blocks)	23	20	21	21	23	22	20	21	21	22	22	22
Group 2 (61 blocks)	15	16	15	16	18	18	22	17	22	21	25	22
Group 3 (50 blocks)	3	4	2	3	5	4	4	8	7	8	8	8
Group 4 (17 blocks)	0	0	0	0	0	0	0	0	0	0	0	0

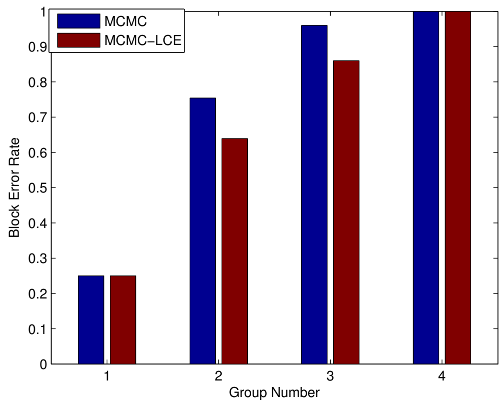

Fig. 7. BLER with single block decoding in each group ($D = 3$)

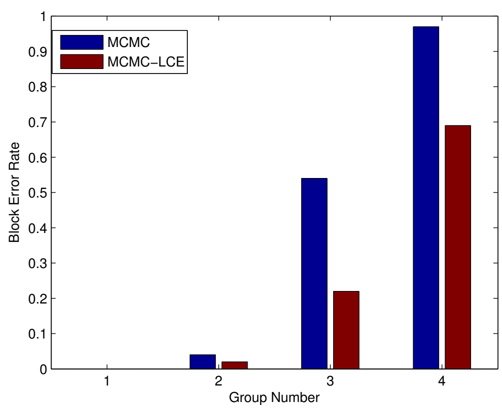

Fig. 8. BLER when combining two blocks within each group ($D = 3$)

V. CONCLUSION

In this paper, we proposed to use the instantaneous channel estimate to determine the channel delay and Doppler spreads, and categorized the channel conditions based on the estimated Doppler spread. We then presented the MCMC-LCE receiver, targeting channels with large Doppler spreads. Data sets collected in a swimming pool with a mobile node at different speeds were used for channel classification and receiver performance validation. The Doppler spread estimate can be used to assist the receiver for performance prediction and receiver configuration.

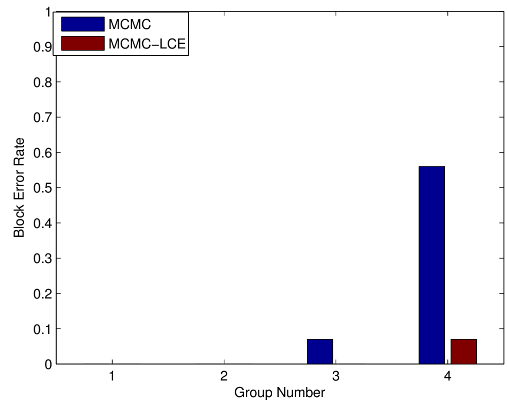

Fig. 9. BLER when combining four blocks within each group ($D = 3$); No decoding error for groups 1 and 2, and for group 3 with MCMC-LCE.

ACKNOWLEDGEMENT

This work was partially supported by the NSF grants PLR-1344264 and ECCS-1310406. S. Zhou has an ownership interest in AquaSeNT, which is a marine sensor and communication technology firm that develops underwater wireless communication technology.

REFERENCES

[1] K. Tu, T. Duman, M. Stojanovic, and J. Proakis, “Multiple-resampling receiver design for OFDM over Doppler-distorted underwater acoustic channels,” *IEEE J. Ocean. Eng.*, vol. 38, no. 2, pp. 333-346, Apr. 2013.

[2] J.-Z. Huang, S. Zhou, and Z.-H. Wang, “Performance results of two iterative receivers for distributed MIMO-OFDM with large Doppler deviations,” *IEEE J. of Oceanic Engr.*, vol. 38, no. 2, Apr. 2013.

[3] H. Wan, R.-R. Chen, J. W. Choi, A. Singer, J. Preisig, and B. Farhang-Boroujeny, “Markov chain Monte Carlo detection for frequency-selective channels using list channel estimates,” *IEEE J. Sel. Top. Signal Process.*, vol. 5, no. 8, pp. 1537-1547, Dec. 2011.

[4] C. R. Berger, S. Zhou, J. C. Preisig, and P. Willett, “Sparse channel estimation for multicarrier underwater acoustic communication: From subspace methods to compressed sensing,” *IEEE Transactions on Signal Processing*, vol. 58, no.3, pp. 1708-1721, Mar. 2010.

[5] J.-Z. Huang, S. Zhou, J. Huang, C. R. Berger, and P. Willett, “Progressive inter-carrier interference equalization for OFDM transmission over time-varying underwater acoustic channels,” *IEEE Journal of Selected Topics in Signal Processing*, vol. 5, no. 8, pp. 1524-1536, Nov. 2011.

[6] Y. Huang, L. Wan, S. Zhou, Z.-H. Wang and J.-Z. Huang, “Comparison of Sparse Recovery Algorithms for Channel Estimation in Underwater Acoustic OFDM with Data-Driven Sparsity Learning,” *Elsevier Journal on Physical Communication*, Aug. 2014.

[7] J. Ling and J. Li, “Gibbs-sampler-based semiblind equalizer in underwater acoustic communications,” *IEEE Journal of Oceanic Engineering*, vol. 37, no. 1, pp. 1-13, Jan. 2012.

[8] S. J. Wright, R. D. Nowak, and M. A. Figueiredo, “Sparse reconstruction by separable approximation,” *IEEE Trans. Signal Processing*, vol. 57, no. 7, pp. 24792493, July 2009.